Surface & Coatings Technology 349 (2018) 1069–1076

Contents lists available at ScienceDirect

Surface & Coatings Technology

journal homepage: www.elsevier.com/locate/surfcoat

Corrosion characteristics and wear performance of cold sprayed coatings of reinforced Al deposited onto friction stir welded AA2024-T3 joints

Na Li[a,b], Wenya Li[a,*], Xiawei Yang[a], Yaxin Xu[a], Achilles Vairis[a,c]

[a] State Key Laboratory of Solidification Processing, Shaanxi Key Laboratory of Friction Welding Technologies, Northwestern Polytechnical University, Xi'an 710072, PR China
[b] Shaanxi Railway Institute, Weinan 714000, Shaanxi Province, PR China
[c] Department of Mechanical Engineering, TEI of Crete, Heraklion, Crete 71004, Greece

ARTICLE INFO

Keywords:
Friction stir welding
Cold spraying
Aluminum coating
Corrosion
Wear

ABSTRACT

A pure Al coating and Al based composite coating reinforced with 20 vol% Al_2O_3 particles were deposited onto a friction stir welded AA2024-T3 joint substrate. The effects of hard Al_2O_3 particles on the coating microstructure, electrochemical behavior and wear performance were investigated. Microstructural analysis shows that the addition of ceramic particles enhances the coating density. Results of electrochemical tests show that both the Al-20 vol% Al_2O_3 composite coating and pure Al coating provide cathodic protection to the friction stir welded joint substrate. The Al-20 vol% Al_2O_3 composite coating shows higher corrosion current density than the pure Al coating due to the inter-particle (between Al_2O_3 and Al particles) boundaries and the severer plastic deformation of Al particles accelerating the corrosion reaction. The presence of Al_2O_3 particles in Al matrix improves the coating wear resistance and changes the wear mode from abrasive wear to adhesive one when compared to the unreinforced pure Al coating.

1. Introduction

The 2xxx series aluminum alloys are promising lightweight materials used in engineering applications, such as automotive, aerospace, shipbuilding and electronic industries for their low cost, low density, fairly high strength, fracture toughness and excellent workability [1, 2]. However, these high strength aluminum alloys are difficult-to-weld with conventional fusion welding as they are prone to form poor dentritic solidification microstructures and develop pores and cracks which greatly deteriorate joint mechanical properties [3, 4].

Friction stir welding (FSW), an innovative solid-state welding technique, was developed at The Welding Institute (TWI) of the United Kingdom in 1991 and was initially used for aluminum alloys. Nowadays, FSW has expanded to join all series aluminum alloys and magnesium alloys. Furthemore, the feasibility of FSW for steels, Ti alloys, and Ni-base superalloys has been demonstrated [5–7]. FSW uses the combined effects of frictional heat and plastic strain which are generated by stirring between the tool shoulder and the top of the sheets being welded [8, 9]. However, these thermo-mechanical conditions introduce a large variation of microstructures and mechanical properties throughout the joint [10]. A typical FSW joint of aluminum alloys can be divided into four distinct microstructural zones: the stirred zone (SZ), the thermo-mechanically affected zone (TMAZ), the heat-affected zone (HAZ) and the base material (BM) [11]. Where there is an Al clad layer for corrosion protection, it is broken by the severe mechanical action of the rotating tool shoulder [12], which removes the corrosion protection of Al clad layer for the joint being friction stir welded. Published works on the corrosion behavior of joints have identified that the welded regions were more susceptible to localized corrosion than the BM itself [1, 13]. This suggests that the major problem for the friction stir welded aluminum alloy joints is the corrosion susceptibility.

Up to now, there have been a limited number of investigations on improving the joint corrosion resistance by lowering heat input during welding (using cryogenic cooling, spraying water on the tool, or selecting welding parameters and so on), post-weld heat treatments, surface modification (laser surface melting (LSM) and micro-arc oxidation (MAO)) and spray coatings (thermal spraying (TS)) [14–21]. Of these, the former two methods can improve to a limited extent the joint corrosion resistance by lowering heat input during FSW [14, 15]. Due to the development of residual stresses during FSW and the steep microstructure gradient formed following heat treatment, corrosion cannot be completely eliminated [16, 17]. With the latter two methods, surface treated layers or coatings provide better protection for the

* Corresponding author.
E-mail address: liwy@nwpu.edu.cn (W. Li).

https://doi.org/10.1016/j.surfcoat.2018.06.058
Received 24 December 2017; Received in revised form 2 April 2018; Accepted 24 June 2018
Available online 26 June 2018

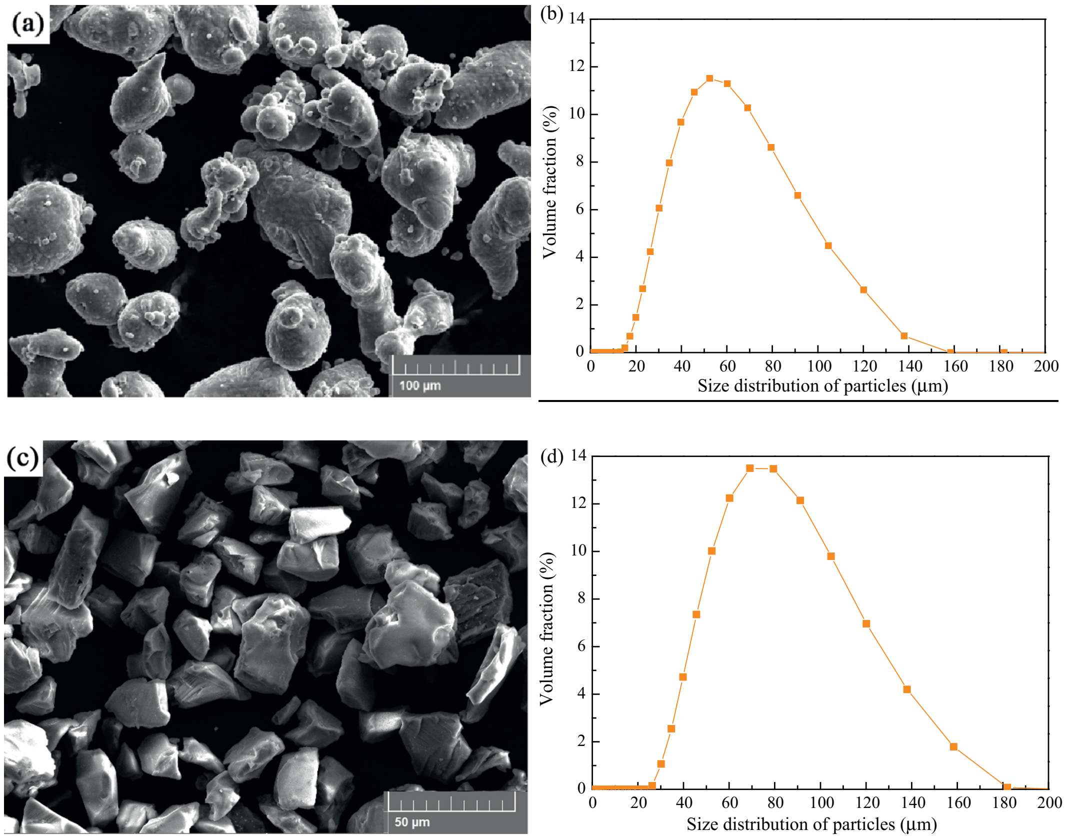

Fig. 1. SEM morphologies of (a) Al powder and (c) Al_2O_3 powder; size distributions of (b) Al powder and (d) Al_2O_3 powder.

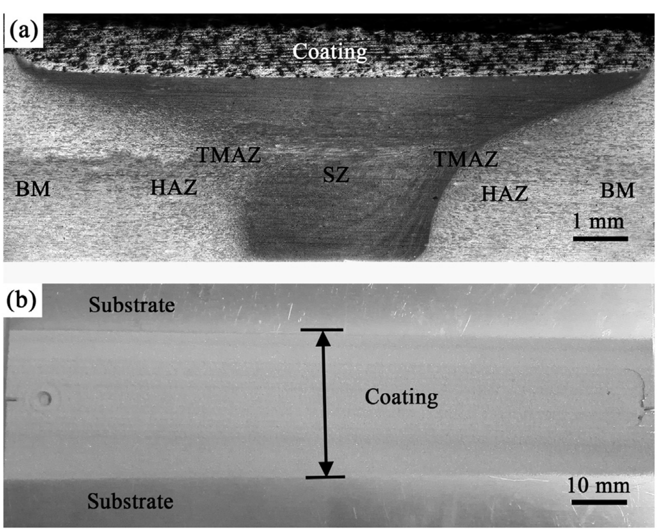

Fig. 2. Cross-sectional OM (a) and photo (b) of the Al-20 vol% Al_2O_3 coating on the joint.

friction stir welded joints. At the same time they have certain disadvantages, such as the LSM layer which undergoes partial delamination and element concentration [18], and an MAO layer having a porous surface which requires post-sealing while deteriorating the mechanical properties of the joint [20]. TS coatings with post-sealing treatment seem to provide good protection [21]. Nevertheless, the relatively high temperature heating during the TS process may lead to distortion of joints. Consequently, the TS technique is rarely used for surface protection of friction stir welded Al alloy joints.

Cold spraying (CS) is a novel solid-state technique that produces improved bonds, does not lead to phase transformation, has lower porosity and develops residual compressive stress, which are unattainable with the conventional TS technologies [22–24]. These features make the CS an appropriate technique to create dense coatings without oxidation, phase transformation or atom diffusion into the substrate, which enable the feedstock powders to retain their original properties [25, 26]. CS has been used to fabricate coatings with corrosion, wear, repair and high temperature resistance, as well as functional coatings for industrial applications [25–30]. Furthermore, CS has the ability to join dissimilar metals (e.g. Al and Mg), but it is still a challenge due to the formation of brittle intermetallic compounds [31]. Aluminum coatings have been a good alternative for corrosion protection of friction stir welded joints. In recent years, only Trahan [32] and Li [33] have deposited pure Al coatings by CS on the surfaces of friction stir welded Al alloy joints and assessed their corrosion performance. Results showed that the corrosion resistance of the friction stir welded joints were greatly improved.

It is well known that the inclusion of ceramic particles as reinforcement can improve mechanical properties of metal matrix composites [34, 35]. To further improve the performance of cold sprayed coatings, hard particles at different ratios have been introduced into the feedstock to fabricate composite coatings [36–38]. The deposition efficiency and bond strength of the coating to the substrate can be improved by adding reinforcements to a metal powder with the appropriate proper proportion [38]. In addition, a number of cold sprayed Al-Al_2O_3 coatings have been deposited on carbon steel or other light alloys substrates [39, 40]. To the authors' best knowledge, the corrosion behavior and wear resistance of the cold sprayed Al_2O_3 reinforced aluminum composite coatings on the friction stir welded joints have not been studied. It is therefore, the purpose of this study to investigate the effect of 20 vol% Al_2O_3 on the microstructure, corrosion performance and wear resistance of the cold sprayed composite coatings.

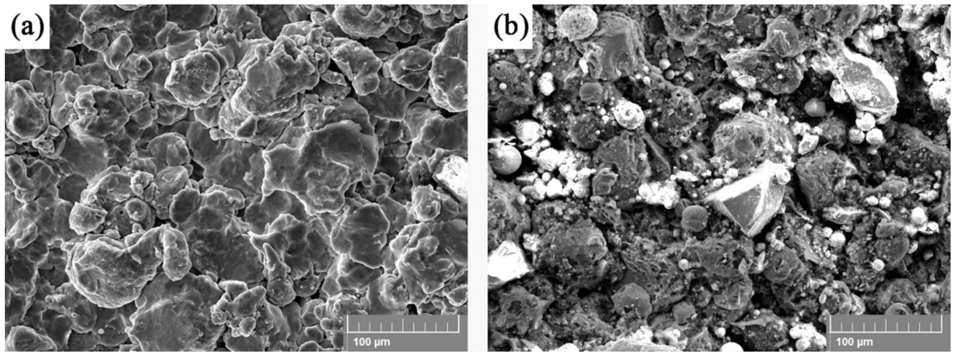

Fig. 3. SEM morphologies of top surfaces of (a) pure Al coating and (b) Al-20 vol% Al_2O_3 composite coating.

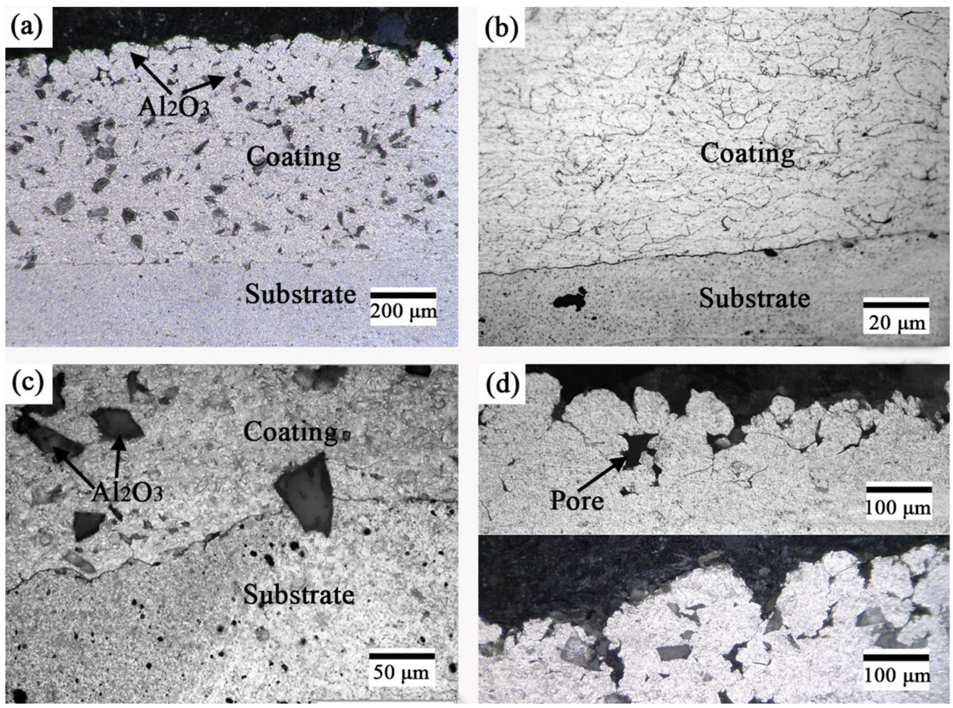

Fig. 4. Cross-sectional OM images of the coatings: (a) Al-20 vol% Al_2O_3 composite coating, (b) Al coating, (c) high magnification of coating-substrate interface of Al-20 vol% Al_2O_3 composite coating, and (d) high magnification of top layers of Al coating (upper) and Al-20 vol% Al_2O_3 composite coating (lower).

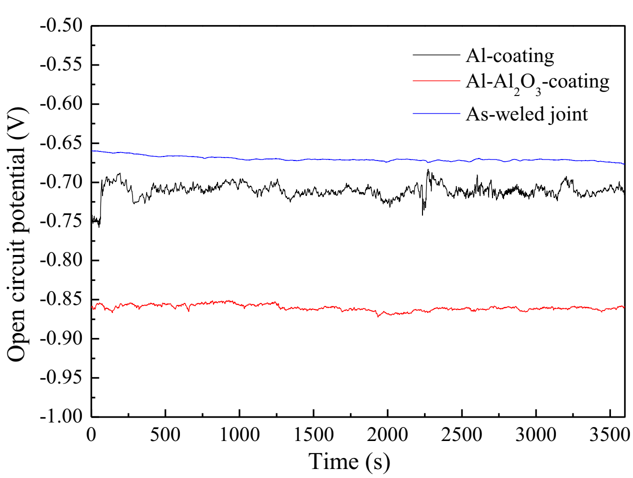

Fig. 5. Open circuit potential vs time for all samples measured in 3.5 wt% NaCl solution for 1 h at 25 °C.

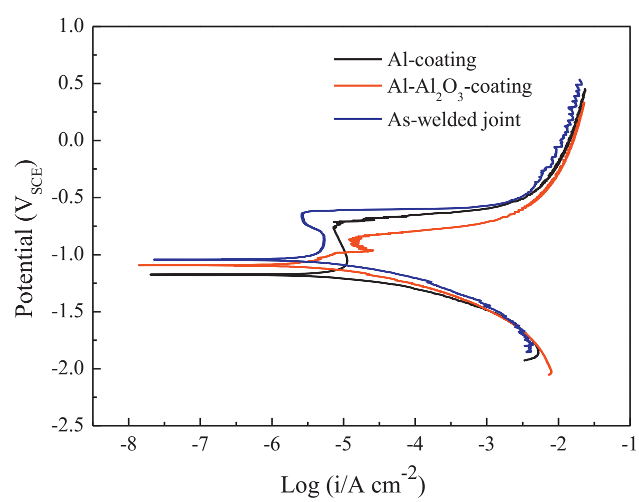

Fig. 6. Potentiodynamic polarization curves of all samples in 3.5 wt% NaCl solution.

Table 1
Corrosion parameters estimated from potentiodynamic polarization curves.

Sample	Friction stir welded joint	Al coating	Al-Al_2O_3 coating
E_{cor}(vs SCE)/V	−1.018	−1.170	−1.033
E_{pit}(vs SCE)/V	−0.743	−0.752	−0.851
i_{cor}/(μA·cm^{-2})	10.495	8.526	12.865

2. Experimental procedure

2.1. Materials

3.2 mm AA2024-T3 aluminum alloy sheets with a length of 200 mm and width of 100 mm were butt-welded by a commercial FSW machine (FSW-RL31-010, Beijing FSW Technology Co., Ltd.). The welds were parallel to the rolling direction of the sheets (length direction). The friction stir tool had a right-hand threaded conical probe of 3.4 mm in diameter and 2.9 mm in length and a concave shoulder of 10 mm in diameter. The optimum welding parameter was selected based on our previous study at a rotation speed of 600 rpm and traveling speed of 200 mm/min [41].

The friction stir welded AA2024-T3 joint was then used as the substrate material in CS. In order to keep the original joint surfaces, sand-blasting was not conducted but the joints were rinsed with acetone to remove any adsorbed contaminants. The feedstock powders used in CS were composed of a gas-atomized aluminum powder as the matrix and 20 vol% commercially available Al_2O_3 powder as the reinforcement. They were mechanically blended. A CS system developed in the Xi'an Jiaotong University of China was used for coating deposition. The nozzle had an expansion ratio of 4.9 and a divergent section length of 170 mm. Nitrogen was used as the accelerating gas at an inlet pressure of 2.8 MPa and temperature of around 450 °C. The powder feeding rate is 2 rad/min. The nozzle standoff distance from the friction stir welded joint surface was set as 30 mm and the nozzle traverse speed was set as 60 mm/min. The coatings were deposited in four passes during the CS process.

2.2. Test methods

The metallographic observation of the coating and substrate on the transverse cross-section was conducted with an optical microscope (OM, OLYMPUS GX71, Japan). Samples were embedded in a resin, progressively ground with SiC abrasive papers from P400 to P3000 size, polished with a 1.5 μm diamond paste and finally etched with a Dix-Keller's reagent. A scanning electron microscope (SEM, JSM5800LV, JEOL, Japan) was used to characterize the top surface morphologies of the coatings.

Electrochemical measurements were used to characterize the corrosion performance of the coatings on the friction stir welded joints. Before electrochemical testing, all samples were rinsed in an ultrasonic bath with acetone and mechanically ground up to 3000 grit followed by polishing with a 1.5 μm diamond paste to obtain a scratch free surface. The electrolyte was a non-deaerated and unstirred 3.5 wt% NaCl aqueous solution which was maintained at 25 °C. The friction stir welded AA2024-T3 joint was also tested as a reference. A standard three-electrode electrochemical cell was used for testing. The cold sprayed coating was used as the working electrode with 0.2 cm^2 immersed in the solution. The counter electrode was a platinum sheet and the potential was referred to a standard calomel electrode connected to the working solution through a Luggin capillary. Samples were immersed in the solution for 1 h to reach the steady state potential. Potentiodynamic scans were performed from −1.2 V to +1.2 V vs open circuit potential (OCP) at a scan rate of 0.167 mV/s.

Dry sliding wear tests on the pure Al and Al-20 vol% Al_2O_3 composite coatings were conducted in a ball-on-disc tribometer (GHT-1000, China) at room temperature in dry air with a load of 2 N, a track radius of 3 mm and a rotation speed of 360 rpm for 20 min. Before the wear tests, all samples were also polished as the corrosion samples. The counter material was a 4 mm ball made of GCr15 steel. Friction coefficients and sliding times were automatically recorded. Finally, the worn traces were observed with SEM.

2.3. Powder and joint characterizations

Pure Al powder presents an irregular or near-spherical shape as shown in Fig. 1a with an average size of 53 μm (Fig. 1b) (Beijing You Xing Lian Technology Co., Ltd., China). The morphology of Al_2O_3 powder is typically angular with sharp edges (Fig. 1c) with an average size of 70 μm (Fig. 1d) (Beijing You Xing Lian Technology Co., Ltd., China). Fig. 2 shows the overview of the typical Al-20 vol% Al_2O_3 coating on the friction stir welded AA2024-T3 joint. It can be clearly seen that the thickness of the Al-20 vol% Al_2O_3 composite coating was about 0.8 mm (Fig. 2a, upper) and the coating width was about 35 mm (Fig. 2b). Therefore, the coating has covered fully the joint zones.

3. Results and discussion

3.1. Microstructure

Fig. 3 shows the SEM morphologies of the top surfaces of the as-sprayed coatings. It can be seen that the cold sprayed coating has a relatively rough suface. Due to the subsequent tamping and rebound action of particles, Al particles seem to be flattened (Fig. 3a). Because of the Al_2O_3 reinforcement, it seems that Al particles undergo stronger tamping effect and deformation [26, 42]. The hard Al_2O_3 particles keep their original morphology (Fig. 3b).

Fig. 4 shows the cross-sectional OM images of pure Al and Al-20 vol

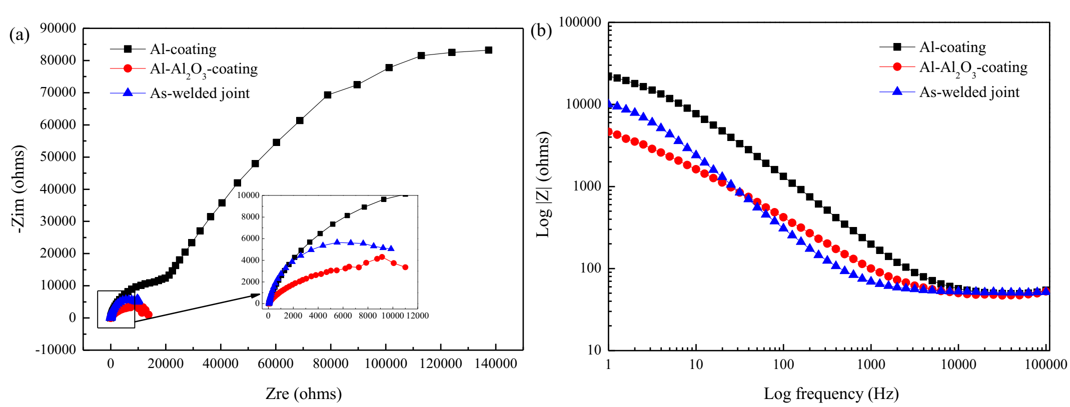

Fig. 7. Nyquist plots of all samples in 3.5 wt% NaCl solution (a) and corresponding Bode plots (b).

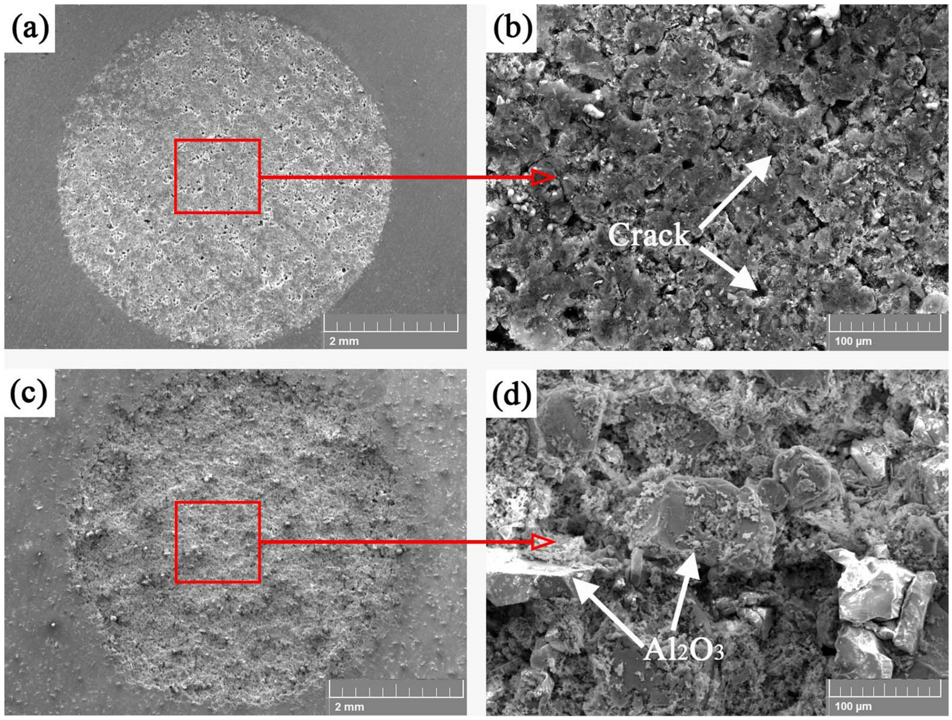

Fig. 8. SEM morphologies of (a, b) pure Al coating and (c, d) Al-20 vol% Al_2O_3 composite coating after electrochemical tests in 3.5 wt% NaCl solution.

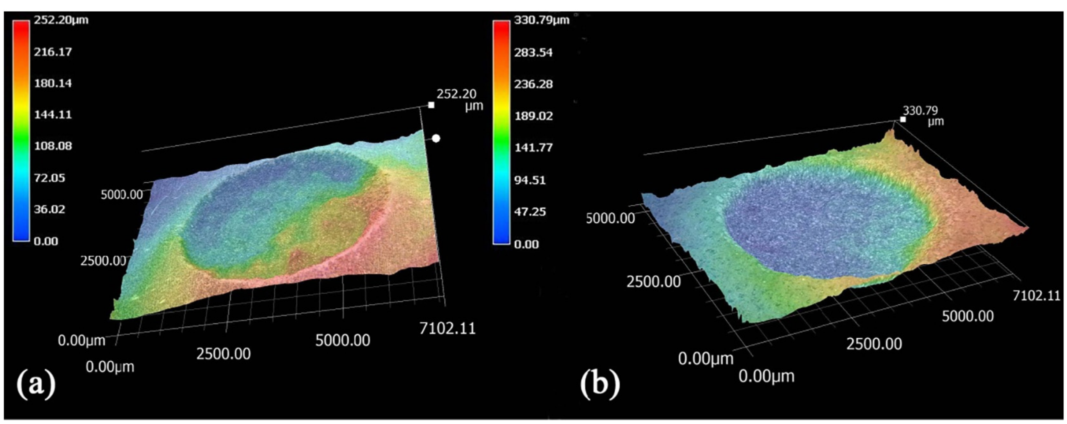

Fig. 9. Three-dimensional topographies of electrochemical specimens: (a) pure Al coating and (b) Al-20 vol% Al_2O_3 composite coating.

% Al_2O_3 composite coatings deposited on friction stir welded AA2024-T3 joints. Fig. 4a and c show that Al particles plastically deform with tamping of the subsequent Al particles and hard Al_2O_3 phase, while cracks and interconnected porosity are not observed at the interface (Fig. 4c) or along the coating thickness (Fig. 4a). It should be noted that the sizes of the Al_2O_3 particles in the composite coating are smaller than the initial powder, which suggests that some of the Al_2O_3 particles have been broken upon impact [42, 43]. It is seen from Fig. 4b that there is no evidence of porosity in the Al coating and it is well bonded to the joint surface. However, in the top region of the coatings, there are a few pores (Fig. 4d), which is expected due to the less deformation [39]. It should be pointed out that the coatings have a denser microstructure, and no pores throughout the whole coating, which means the coatings can isolate the substrate from the electrolyte.

3.2. Eletrochemical corrosion studies

Fig. 5 shows the evolution of OCP vs time in aerated and unstirred 3.5 wt% NaCl solution for the friction stir welded AA2024-T3 joint and coatings. The OCP curves were measured when the OCP steady state was reached after 1 h of immersion. For the two coatings the OCP values are completely different from that of the friction stir welded AA2024-T3 joint. The OCP values of the welded joint maintained almost −0.66 V during the time course of the experiment. For the Al and Al-20 vol% Al_2O_3 coatings the OCP values are completely different from the welded joint. The OCP values tend to stabilize for Al (−0.70 V) and Al-20 vol% Al_2O_3 (−0.84 V) coatings at more negative values than the welded joint. Therefore, the Al and Al-20 vol% Al_2O_3 composite coatings can provide cathodic protective of the sacrificial anode for the friction stir welded joint [44].

The response of pure Al, Al-20 vol% Al_2O_3 composite coating and the friction stir welded AA2024-T3 joint under potentiodynamic polarization is shown in Fig. 6 and Table 1. It can be seen that the addition of 20 vol% Al_2O_3 has a significant effect on polarization. The substrate and pure Al coating show a typical passive region with invariable current density, which is independent of the applied potential up to the pitting potential E_{pit} where they form a passive film and protect the substrate and Al coating from corrosion [26, 44]. After forming the

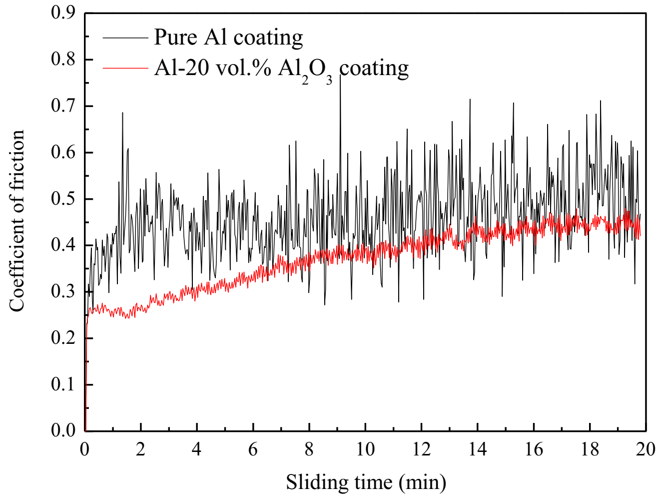

Fig. 10. Coefficient of friction of pure Al coating and Al-20 vol% Al_2O_3 composite coating as a function of sliding time at room temperature.

passive film, the current density increases rapidly because of the destruction of the oxide film by the induced Cl^- ions up to a limit [26]. Following this, the corrosion behavior transits from passive to stable pitting, where the current density increases slightly with potential. The substrate, Al coating and Al-20 vol% Al_2O_3 composite coating show E_{cor} values of −1.018 V, −1.171 V and −1.033 V_{SCE}, respectively. Furthemore, the pit potential and current density are commonly employed to assess the kinetics of corrosion reactions. The i_{cor} value of Al coating (i_{cor} = 8.526 μA/cm^2) is lower than that of Al-20 vol% Al_2O_3 composite coating (i_{cor} = 12.865 μA/cm^2) and the E_{pit} value of the Al coating shifts to more anodic, which indicates that the Al coating shows a better corrosion resistance than the Al-20 vol% Al_2O_3 composite coating. This is consistent with the SEM morphologies after corrosion tests.

Fig. 7 shows EIS diagrams that illustrate the impedance behavior of Al and Al-20 vol% Al_2O_3 coatings in 3.5 wt% NaCl solution at 25 °C, which demonstrate corrosion tendency. The semicircle radius of the Al coating is greater than that of the Al-20 vol% Al_2O_3 coating. Therefore, the Al coating shows a higher modulus of impedance, as adding Al_2O_3 particles decreases corrosion resistance. It should be noted that the Al and Al-Al_2O_3 coatings are dense and the electrolyte does not reach the substrates. The Niquist and Bode plots are in agreement with potentiodynamic polarization.

For the Al-20 vol% Al_2O_3 composite coating, the Cl^- ions adsorb onto the oxide film, then assist the localized dissolution at specific sites at the Al_2O_3/film or Al_2O_3/Al interface that develop into pits. The pits mainly surrounded the Al_2O_3 particles in the reinforced Al coating. Hence, when the Al_2O_3 particles are inert in the neutral 3.5 wt% NaCl solution, the defects around the Al_2O_3 particles and Al matrix are the main sites for pitting initiation and the attack can be higher around the Al_2O_3 particles. Moreover, the more active sites for corrosion induced by the high severe plastic deformation is another reason for lower corrosion resistance of the Al-20 vol% Al_2O_3 composite coating.

3.3. Morphology of corrosion attack

Fig. 8 shows the surface morphology of the two coatings after polarization test in the 3.5 wt% NaCl solution. The surface of Al and Al-Al_2O_3 coatings reveal a high degree of corrosion. The examination of EDS (not shown) revealed Al, oxygen and chlorine as the constituents of the corrosion products [31]. It can be observed that the Al-Al_2O_3 composite (reinforced) coating is more heavily affected by the corrosion than the pure Al coating. Some uniformly sized deep holes are present on the surface of the Al coating after the polarization test. This corrosion behavior is the result of the porous surface as shown in Fig. 4d, while the coatings do not possess pores through the thickness direction and are impermeable to solution. Compared to the pure Al coating, the Al-Al_2O_3 coating shows stronger corrosion attack, which is caused by the following reasons. The positive factors: the shot-peening effect of Al_2O_3 particles makes the Al particles have higher plastic deformation which induces the lower porosity of composite coatings than that of Al coating [41].

The negative factors are:

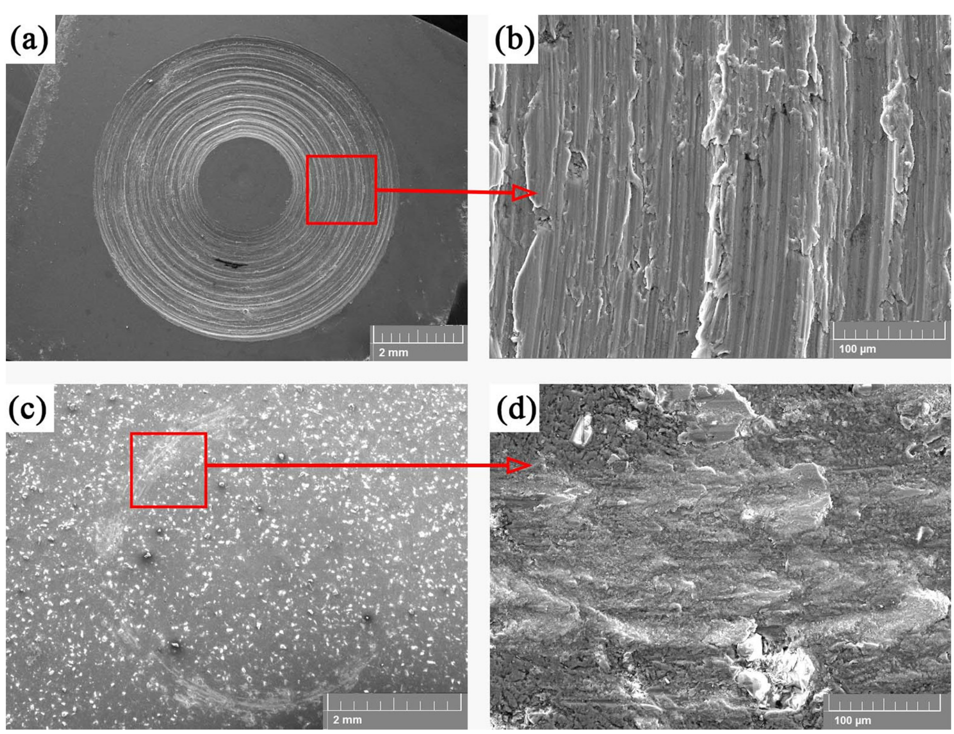

Fig. 11. SEM morphologies of the worn tracks of (a, b) pure Al coating and (c, d) Al-20 vol% Al_2O_3 composite coating.

i) the inter-particles boundaries between Al and Al_2O_3 particle are the main active sites attacked by electrolyte. Wang et al. [44] have reported similar observation for cold sprayed SiC reinforced Al 5056 composite coatings.
ii) the composite coatings have undergone higher severe plastic deformation induced by Al_2O_3 particle in comparison with the unreinforced pure Al coating, which leads to more active sites for corrosion. Futhermore, the residual stress generation during spray deposition also leads to a higher rate of corrosion [45]. Meydanoglu et al. [46] showed that the SiC particles increased corrosion current densities of the reinforced Al 7075 coating due to the internal stresses.

If the effect is dominated by the negative factors, the corrosion resistance will be decreased for the composite coating. In this study, the negative factors are dominant. Therefore, some deep holes around the interface of Al_2O_3 and the Al particles have been formed after polarization test. Moreover, the Al_2O_3 particles are not corroded because of its poor conductor (actually an insulator) and are covered with corrosion products. These are in agreement with the electrochemical test results.

In addition, intense oxygen affinity of Al creates a uniform passive film on the surface of the substrate and Al coating [26, 45]. During the corrosion initial stage, the passive film can cut off Cl^- ions from the electrolyte and impede direct corrosion [39]. With longer immersion time, more Cl^- ions assemble and pass into the matrix through the weak spots, such as the suface pores on the Al and Al-Al_2O_3 coatings. The positive ions of the matrix and the Cl^- ions can form soluble chloride and then start the pitting nuclei. With the dissolution of the matrix metal anode, these pits begin to grow and gradually join together into pit holes. Finally, the pit holes grow even further and expand in the depth direction.

The three-dimensional topographies of electrochemical specimens are shown in Fig. 9. Compared to the Al-20 vol% Al_2O_3 composite coating, a relatively deep corrosion hole has produced in the pure Al coating, which leads to a lower corrosion resistance and has a good agreement with the SEM morphologies after electrochemical tests.

3.4. Wear behavior

Fig. 10 shows a typical measurement of the coefficient of friction (COF) vs sliding time for pure Al coating and Al-20 vol% Al_2O_3 composite coating deposited on a friction stir welded AA2024-T3 joint. The COFs of both coatings show a similar overall behavior. At the initial stage, the COF rises to a higher value which is followed by a steady state due to the change of wear mechanism. At a load of 2 N, the COF of the pure Al coating increases from 0.35 to 0.55, while the Al-20 vol% Al_2O_3 coating has a dramatical drop. It can be concluded that the addition of Al_2O_3 particles greatly affects the wear behavior of the composite coating.

To explain this phenomenon, the worn tracks of the pure Al and Al-20 vol% Al_2O_3 composite coatings are observed and shown in Fig. 11. It can be clearly seen that the worn track of the pure Al coating is wider and deeper than that of the Al-20 vol% Al_2O_3 composite coating, which is associated with the higher wear resistance of the Al-20 vol% Al_2O_3 coating. The appearance of the surface of pure Al coating (Fig. 11a and b) is typical of adhesive wear and the worn material is ploughed and extruded outside the worn track. The loose wear debris have the same color and appearance with the Al coating, again indicating an adhesive wear, where the softer Al coating transfers to the surface of harder counter steel ball. Fig. 11c and d show a worn track of the Al-20 vol% Al_2O_3 coating. The wear surface shows signs of smearing and adhesive wear as in the pure Al coating, but also some evidence of abrasive wear. These wear features indicate that Al_2O_3 particles as a hard phase behave as lubricants reducing wear and changing the wear mode [26, 39]. The higher hardness of a solid can lower in effect its abrasive wear [47], the addition of the higher hardness of Al_2O_3 particles is correlated to the higher abrasive wear resistance of the Al-20 vol% Al_2O_3 coating. Therefore, the wear mechanism is adhesive wear in the Al coating like pure Al bulk. For the Al-20 vol% Al_2O_3 coating, abrasive wear is the mainly mechanism. This transition is reflected by a significant reduction in wear rate of the coating. The wear resistance of the cold sprayed Al-20 vol% Al_2O_3 coating is better than that of the pure Al coating as far as the morphological features of the worn tracks show, which indicate the potential of the Al-20 vol% Al_2O_3 coating for wear protection of the friction stir welded AA2024-T3 joint substrate.

4. Conclusions and outlook

(1) Pure Al or Al-20 vol% Al_2O_3 composite coating has been successfully deposited onto the surface of a friction stir welded AA2024-T3 joint by the CS technique. For both types of coatings, pores always appear at the top surface due to the less tamping effect by the subsequent particles.
(2) Both coatings can provide cathodic protection for the friction stir welded joints. The as-sprayed Al-20 vol% Al_2O_3 reinforced coating shows a lower corrosion resistance compared to the pure Al coating.
(3) The lower corrosion resistance of the Al-20 vol% Al_2O_3 coating is attributed to the presence of more active sites induced by the high severe plastic deformation in comparison with the unreinforced pure Al coating. Moreover, the interfaces between reinforcement and matrix particles are also active sites easily attacked by the electrolyte.
(4) The Al-Al_2O_3 coating has better wear resistance than pure Al coating. Wear morphological features indicate that the wear mode is adhesive wear for the pure Al coating and abrasive wear for the Al-20 vol% Al_2O_3 coating. The wear mode becomes fully abrasive as the wear rate is reduced for the Al-20 vol% Al_2O_3 coating.
(5) The addition of the hard Al_2O_3 phase into Al coating has improved to a limited extent the wear performance at the expense of corrosion resistance. Based on this finding, what is required next is the combination of the improved corrosion resistance of pure Al with the better wear resistance of the Al-20 vol% Al_2O_3 coating. Two coating layers can be deposited onto the surface of the friction stir welded AA2024-T3 joint, the outer layer being the Al-20 vol% Al_2O_3 composite coating while the inner layer would be pure Al coating. This kind of two-layer coating would provide even better mechanical resistance with its reinforced coating on the surface and better corrosion resistance with pure Al in the inner. This will be the topic of our future research.

Acknowledgements

The authors would like to thank for financial support the National Natural Science Foundation of China (51574196), the 111 Project (B08040), the fund of SAST (SAST2016043) and the National Key Research and Development Program of China (2016YFB0701203). The authors also thank Assoc. Prof. Xiaotao Luo and Dr. Yujuan Li from Xi'an Jiaotong University for their help in coating deposition.

References

[1] E. Bousquet, A. Poulon-Quintin, M. Puiggali, O. Devos, M. Touzet, Relationship between microstructure, microhardness and corrosion sensitivity of an AA2024-T3 friction stir welded joint, Corros. Sci. 53 (2011) 3026–3034.
[2] J. Goebel, M. Reimann, A. Norman, J.F.D. Santos, Semi-stationary shoulder bobbin tool friction stir welding of AA2198-T851, J. Mater. Process. Technol. 245 (2017) 37–45.
[3] Z.H. Zhang, W.Y. Li, Y. Feng, J.L. Li, Y.J. Chao, Improving mechanical properties of friction stir welded AA2024-T3 joints by using a composite backplate, Mater. Sci. Eng. A 598 (2014) 312–318.
[4] S.M. Bayazid, H. Farhangi, H. Asgharzadeh, L. Radan, A. Ghahramani, A. Mirhaji, Effect of cyclic solution treatment on microstructure and mechanical properties of friction stir welded 7075 Al alloy, Mater. Sci. Eng. A 649 (2016) 293–300.

[5] S. Sabooni, F. Karimzadeh, M.H. Enayati, A.H.W. Ngan, Friction-stir welding of ultrafine grained austenitic 304L stainless steel produced by martensitic thermo-mechanical processing, Mater. Des. 76 (2015) 130–140.
[6] K. Kitamura, H. Fujii, Y. Iwata, Y.S. Sun, Y. Morisada, Flexible control of the microstructure and mechanical properties of friction stir welded Ti-6Al-4V joints, Mater. Des. 46 (2013) 348–354.
[7] Y.S. Sato, P. Arkom, H. Kokawa, T.W. Nelson, R.J. Steel, Effect of microstructure on properties of friction stir welded Inconel Alloy 600, Mater. Sci. Eng. A 477 (2008) 250–258.
[8] Z.H. Zhang, W.Y. Li, Y. Feng, J.L. Li, Y.J. Chao, Global anisotropic response of friction stir welded 2024 aluminum sheets, Acta Mater. 92 (2015) 117–125.
[9] Z. Zhang, B.L. Xiao, Z.Y. Ma, Hardness recovery mechanism in the heat-affected zone during long-term natural aging and its influence on the mechanical properties and fracture behavior of friction stir welded 2024Al-T351 joints, Acta Mater. 73 (2014) 227–239.
[10] Z.L. Hu, X.S. Wang, S.J. Yuan, Quantitative investigation of the tensile plastic deformation characteristic and microstructure for friction stir welded 2024 aluminum alloy, Mater. Charact. 73 (2012) 114–123.
[11] P.L. Niu, W.Y. Li, Z.H. Zhang, X.W. Yang, Global and local constitutive behaviors of friction stir welded AA2024 joints, J. Mater. Sci. Technol. (9) (2017) 987–990.
[12] Y.M. Yue, Z.W. Li, S.D. Ji, Y.X. Huang, Z.L. Zhou, Effect of reverse-threaded pin on mechanical properties of friction stir lap welded alclad 2024 aluminum alloy, J. Mater. Sci. Technol. 32 (2016) 671–675.
[13] Y. Deng, B. Peng, G.F. Xu, Q.L. Pan, R. Ye, Y.J. Wang, L.Y. Lu, Z.M. Yin, Stress corrosion cracking of a high-strength friction-stir-welded joint of an Al-Zn-Mg-Zr alloy containing 0.25 wt.% Sc, Corros. Sci. 100 (2015) 57–72.
[14] M. Jariyaboon, A.J. Davenport, R. Ambat, B.J. Connolly, S.W. Williams, D.A. Price, Effect of cryogenic cooling on corrosion of friction stir welded AA7010-T7651, Anti-Corros. Methods Mater. 57 (2010) 83–89.
[15] G. İpekoğlu, G. Çam, Effects of initial temper condition and postweld heat treatment on the properties of dissimilar friction-stir-welded joints between AA7075 and AA6061 aluminum alloys, Metall. Mater. Trans. A 45 (2014) 3074–3087.
[16] C.S. Paglia, R.G. Buchheit, The influence of a propane gas torch flame post-weld heat treatment on the mechanical and corrosion properties of a 2219-T87 friction stir weld, Weld. Cut. 6 (2007) 96–102.
[17] C.S. Paglia, K.V. Jata, R.G. Buchheit, The influence of artificial aging on the microstructure, mechanical properties, corrosion, and environmental cracking susceptibility of A 7075 friction-stir-weld, Mater. Corros. 58 (2007) 737–750.
[18] S.J. Kalita, Microstructure and corrosion properties of diode laser melted friction stir weld of aluminum alloy 2024-T351, Appl. Surf. Sci. 257 (2011) 3985–3997.
[19] C. Padovani, A.J. Davenport, B.J. Connolly, S.W. Williams, E. Siggs, A. Groso, M. Stampanoni, Corrosion protection of AA7449-T7951 friction stir welds by laser surface melting with an Excimer laser, Corros. Sci. 53 (2011) 3956–3969.
[20] K.P. Rao, G.D.J. Ram, B.E. Stucker, Improvement in corrosion resistance of friction stir welded aluminum alloys with micro arc oxidation coatings, Scr. Mater. 58 (2008) 998–1001.
[21] A. Pardo, P. Casajús, M. Mohedano, A.E. Coy, F. Viejo, B. Torres, E. Matykina, Corrosion protection of Mg/Al alloys by thermal sprayed aluminium coatings, Appl. Surf. Sci. 255 (2009) 6968–6977.
[22] K. Yang, W.Y. Li, P.L. Niu, X.W. Yang, Y.X. Xu, Cold sprayed AA2024/Al_2O_3 metal matrix composites improved by friction stir processing: microstructure characterization, mechanical performance and strengthening mechanisms, J. Alloys Compd. 736 (2018) 115–123.
[23] G. Goupil, S. Jucken, D. Poirier, J.G. Legoux, E. Irissou, B. Davis, L. Roué, Cold sprayed Cu-Ni-Fe anode for Al production, Corros. Sci. 90 (2015) 259–265.
[24] W.Y. Li, X.P. Guo, C. Verdy, L. Dembinski, H.L. Liao, C. Coddet, Improvement of microstructure and property of cold-sprayed Cu-4 at.% Cr-2 at.% Nb alloy by heat treatment, Scr. Mater. 55 (2006) 327–330.
[25] Y. Tao, T. Xiong, C. Sun, L. Kong, X. Cui, T. Li, G.L. Song, Microstructure and corrosion performance of a cold sprayed aluminium coating on AZ91D magnesium alloy, Corros. Sci. 52 (2010) 3191–3197.
[26] K. Spencer, D.M. Fabijanic, M.X. Zhang, The use of Al-Al_2O_3 cold spray coatings to improve the surface properties of magnesium alloys, Surf. Coat. Technol. 204 (2009) 336–344.
[27] W.Y. Li, K. Yang, S. Yin, X.W. Yang, Y.X. Xu, R. Lupoi, Solid-state additive manufacturing and repairing by cold spraying: a review, J. Mater. Sci. Technol. 34 (2018) 440–457.
[28] V.K. Champagne, M.K. West, M.R. Rokni, T. Curtis, V. Champagne, B. McNally, Joining of cast ZE41A Mg to wrought 6061 Al by the cold spray process and friction stir welding, J. Therm. Spray Technol. 25 (2016) 143–159.
[29] V.K. Champagne, The Cold Spray Materials Deposition Process: Fundamentals & Applications, Woodhead Publishing Limited, Abington Hall, Cambridge CB21 6AH, England, 2007.
[30] C.M. Kay, J. Karthikeyan, High Pressure Cold Spray, Asm International, 2016.
[31] V. Champagne Jr, D. Kaplowitz, V.K. Champagne, C. Howe, M.K. West, B. McNally, M. Rokni, Dissimilar metal joining and structural repair of ZE41A-T5 cast magnesium by the cold spray (CS) process, Mater. Manuf. Process. 33 (2018) 130–139.
[32] P. Trahan, Corrosion protection of friction stir welded Al 7075 panels using cold gas dynamic spray, The 2013 International Thermal Spray Conference, Busan, May 2013.
[33] W.Y. Li, R.R. Jiang, C.J. Huang, Z.H. Zhang, Y. Feng, Effect of cold sprayed Al coating on mechanical property and corrosion behavior of friction stir welded AA2024-T351 joint, Mater. Des. 65 (2015) 757–761.
[34] X.P. Guo, G. Zhang, W.Y. Li, G. Yang, H.L. Liao, C. Coddet, Investigation of the microstructure and tribological behavior of cold-sprayed tin-bronze-based composite coatings, Appl. Surf. Sci. 255 (2009) 3822–3828.
[35] W.Y. Li, C. Zhang, H.L. Liao, J. Li, C. Coddet, Characterizations of cold-sprayed nickel-alumina composite coating with relatively large nickel-coated alumina powder, Surf. Coat. Technol. 202 (2008) 4855–4860.
[36] P.C. King, S.H. Zahiri, M. Jahedi, Focused ion beam micro-dissection of cold-sprayed particles, Acta Mater. 56 (2008) 5617–5626.
[37] J. Villafuerte, Modern Cold Spray, Springer International Publishing, 2015.
[38] M. Yu, W.Y. Li, X.K. Suo, H.L. Liao, Effects of gas temperature and ceramic particle content on microstructure and microhardness of cold sprayed SiCp/Al 5056 composite coatings, Surf. Coat. Technol. 220 (2013) 102–106.
[39] F.S.D. Silva, J. Bedoya, S. Dosta, N. Cinca, I.G. Cano, J.M. Guilemany, A.V. Benedetti, Corrosion characteristics of cold gas spray coatings of reinforced aluminum deposited onto carbon steel, Corros. Sci. 114 (2017) 57–71.
[40] D. Dzhurinskiy, E. Maeva, E. Leshchinsky, R.G. Maev, Corrosion protection of light alloys using low pressure cold spray, J. Therm. Spray Technol. 21 (2012) 304–313.
[41] W.Y. Li, N. Li, X.W. Yang, Y. Feng, A. Vairis, Impact of cold spraying on microstructure and mechanical properties of optimized friction stir welded AA2024-T3 joint, Mater. Sci. Eng. A 702 (2017) 73–80.
[42] D. Cong, Z. Li, Q. He, H. Chen, Z. Zhao, L. Zhang, H. Wu, Wear behavior of corroded Al-Al_2O_3 composite coatings prepared by cold spray, Surf. Coat. Technol. 326 ((2017) 247–254.
[43] J.M. Shockley, S. Descartes, P. Vo, E. Irissou, R.R. Chromik, The influence of Al_2O_3 particle morphology on the coating formation and dry sliding wear behavior of cold sprayed Al-Al_2O_3 composites, Surf. Coat. Technol. 270 (2015) 324–333.
[44] Y. Wang, B. Normand, N. Mary, M. Yu, H. Liao, Effects of ceramic particle size on microstructure and the corrosion behavior of cold sprayed SiC p/Al 5056 composite coatings, Surf. Coat. Technol. 315 (2017) 314–325.
[45] K. Balani, T. Laha, A. Agarwal, J. Karthikeyan, N. Munroe, Effect of carrier gases on microstructural and electrochemical behavior of cold-sprayed 1100 aluminum coating, Surf. Coat. Technol. 195 (2005) 272–279.
[46] O. Meydanoglu, B. Jodoin, E.S. Kayali, Microstructure, mechanical properties and corrosion performance of 7075 al matrix ceramic particle reinforced composite coatings produced by the cold gas dynamic spraying process, Surf. Coat. Technol. 235 (2013) 108–116.
[47] N.W. Khun, A.W.Y. Tan, K.J.W. Bi, E. Liu, Effects of working gas on wear and corrosion resistances of cold sprayed Ti6Al4V coatings, Surf. Coat. Technol. 302 (2016) 1–12.